# Computational Method for Optimization of Structural Shapes

J. W. Hou,* J. L. Chen,† and J. S. Sheen†
*Old Dominion University, Norfolk, Virginia*

**In the direct method of shape optimum design, mesh regridding is a necessary step in avoiding the distortion of finite element grids. The effect of internal-nodal movements on the shape design sensitivity associated with the regridding process has been carefully examined in this paper. It shows that to maintain computational accuracy, the effects of internal-nodal movement should be considered in shape design sensitivity analysis. To take the internal-nodal movement into account, the numerical accuracy of the speed method is investigated. A new approach, which constructs the velocity field over the element domain, is presented. Although it takes more computational time, the new approach does improve the accuracy of shape design sensitivity.**

## I. Introduction

DESIGN sensitivity analysis studies the effect of change of design variables on the response measures of structural systems. The design variables may be thickness, length, Young's modulus, etc. The response measures may be displacement, stress, temperature distribution, etc. The shape design sensitivity analysis concerns situations in which the shapes of structural components are taken as design variables. Design sensitivity analysis provides a very useful tool to engineers, who can predict the effect of design change based on design sensitivity information. It is also known that sensitivity analysis plays an important role in the iterative optimum design scheme.

In the literature, there are three approaches commonly used to perform the shape design sensitivity analysis, i.e., the direct difference approach,[1] the finite dimensional approach,[2,3] and the material derivative (or speed) method.[4,5] Once the shape design sensitivity is calculated, any gradient-based optimization algorithm can then be used to determine the optimum shape iteratively. One important feature for such an iterative shape optimum scheme is the rearrangement of the finite element mesh. At each iteration, the location of internal nodes will be relocated so that the distortion of the finite element mesh can be avoided. Such nodal relocation can be determined by the meshing optimization algorithm or certain strategies provided by the designer according to the perturbation of the design variables defined along the boundary. To take the effect of internal-nodal movements into account, the numerical accuracy of the speed method will be investigated, and a new approach is also included to improve the speed method for the calculation of shape design sensitivity in this presentation.

To consider the shape change of the domain, one may introduce a time parameter $t$ into the domain deformation process to trace the motion of the particle within the domain. In other words, the new position $x_0$ of any particle in the domain can be expressed as a function of its original position $x$ and time parameter $t$. This is, of course, similar to the material description in the continuum mechanics:

$$x(t) = x(x_0, t)$$

and

$$\dot{x} = \left.\frac{dx}{dt}\right|_{t=0} = v(x_0) \tag{1}$$

where $v(x_0)$ is the velocity.

Since the solution of state equations varies due to the change of boundary shapes, the state variable $z$ depends on the time parameter explicitly as well, i.e.,

$$z(x, t) = z(x(t), t)$$

Assuming $t=0$ to correspond to the undeformed state, the first-order time derivative of $z$ evaluated at the undeformed state is given as

$$\dot{z} = \left.\frac{dz}{dt}\right|_{t=0} = z' + \nabla z^T v \tag{2}$$

where $z' = \partial z/\partial t$ is the time derivative while the position is held fixed, and the "velocity" $v(x)$ is the time derivative of $x(t)$ at $t=0$. The term $\nabla z^T v$ is the contribution of the particle "motion" to the change of state variable.

The foregoing derivative is very similar to the classical general variation of the calculus of variations.[6] The general variation deals with the variation of a functional defined on a variable domain, allowing the state variable $z$ as well as the independent variable $x$ (and hence the domain of state equation) to vary. The principal linear parts (relative to $t$) $\delta x$ and $\delta z$ of the increments $x(t) - x_0$ and $z(x(t), t) - z(x_0)$ are $\delta x = v(x_0)$ and $\delta z = \dot{z}(x_0)$.

The material derivative of a domain integral

$$\psi = \int_\Omega F(z)\,d\Omega$$

according to Eqs. (1-2), can be shown as[5,7]

$$\dot{\psi} = \int_\Omega (\dot{F} + F\,\mathrm{div} v)\,d\Omega = \int_\Omega \left(\frac{\partial F}{\partial z}\dot{z} + F\,\mathrm{div} v\right) d\Omega \tag{3}$$

$$\dot{\psi} = \int_\Omega \left\{\frac{\partial F}{\partial z}z' + \left[\left(\frac{\partial F}{\partial z}\nabla z\right)^T v + F\,\mathrm{div} v\right]\right\} d\Omega = \int_\Omega \left(\frac{\partial F}{\partial z}z'\right) d\Omega + \int_\Gamma FVn\,ds \tag{4}$$

Presented as Paper 85-0773 at the AIAA/ASME/ASCE/AHS 26th Structures, Structural Dynamics and Materials Conference, Orlando, FL, April 15-17, 1985; received April 23, 1985; revision received Sept. 9, 1985. 

*Assistant Professor, Mechanical Engineering and Mechanics.
†Graduate Student, Mechanical Engineering and Mechanics.

where $Vn = v^T n$ is the normal component of the design velocity along boundary $\Gamma$ and div $v$ denotes the divergence of $v$. The last equality is found from an application of the divergence theorem that requires that $Fv$ be continuously differentiable.[8] If such a requirement of regularity is not fulfilled, Eq. (4) should be modified to include an extra term that consists of the jump of $Fv$ defined along the interface where discontinuity happens.

It is important to note that, in general, not only do the discontinuities of function $F$ occur in the shape optimization formulation but the location possessing discontinuities of function $F$ also move in the iterative shape optimization algorithm. As an example, in the problem of shape optimum design of an elastic hollow bar, the torsional rigidity $K$ is considered as the cost function,

$$K = \int_\Omega e^T \nabla z \, d\Omega$$

where $e$ is the position vector and $\nabla z$ is the gradient of stress function. It is clear that the term of $e^T \nabla z$ will have discontinuities across the element boundaries if the finite element displacement method is used for analysis of stress function $z$. Furthermore, it is known that mesh regridding is a necessary step in the direct method of shape optimization, in order to avoid the distortion of finite element grids. At each iteration, the locations of internal nodes will move according to the perturbation of the design variables defined along the boundary. Of course, such nodal movements will change the positions where the discontinuities of $e^T \nabla z$ occur.

To take the discontinuities and the nodal movements into account, an improved computational method for shape optimization is presented in the next section.

## II. Finite Element Method and Speed Method

As discussed in the preceding section, there are two important ingredients in a shape optimum design algorithm, i.e., finite element discretization and mesh regridding. The former introduces discontinuities of function across the element boundaries; the latter makes those discontinuities move. Thus, the nonzero term $Fv$ in the derivation of Eq. (4) is not continuous across the boundary elements, and Eq. (4) cannot be directly applied without modification.

The idea of material derivative is still applicable. However, instead of employing the material derivative for the whole domain, it is proposed that it be used only for each individual finite element. To this end, it is found that Eq. (3) is more useful than Eq. (4) since it is difficult to obtain the value of $z'$ along the element boundaries. There is a significant difference between Eqs. (3) and (4) with respect to the velocity field. The velocity field in Eq. (3) is defined at every point within the domain but is defined only on the boundary in Eq. (4).

Methods for computing the distributed velocity field over the whole domain have been proposed by Cea[9] and Rousselet.[10] Angrand,[11] Haug et al.,[7] and Choi and Seong[12] have also employed a formula similar to Eq. (3) to compute the domain variation. However, the effect of internal-nodal movements on the shape design sensitivity has not been discussed in the literature. In the following derivation, Eq. (3) will be applied to attain the domain variation for all discretized elements in the domain.

The shape optimization of a grooved hollow shaft will be used as a model example here. The torsional rigidity is given by

$$K = \int_\Omega e^T \nabla z \, d\Omega \tag{5}$$

And Clapeyron's theorem yields the following equality for the torsional stress function $z$,[13]

$$\int_\Omega \nabla z^T \nabla z \, d\Omega + \int_\Omega e^T \nabla z \, d\Omega = 0 \tag{6}$$

where $z$ is zero on $\Gamma_0$ and is an arbitrary constant on $\Gamma_i$. After finite element discretization, Eqs. (5) and (6) can be rewritten as

$$K = \sum_1^n \int_{\Omega_i} e^T \nabla z \, d\Omega_i$$

and

$$\sum_1^n \int_{\Omega_i} (\nabla z^T \nabla z + e^T \nabla z) \, d\Omega_i = 0$$

where $n$ is the number of finite elements and $\Omega_i$ is the area of $i$th element. Taking the material derivatives of preceding formulas by using Eq. (3) yields

$$\dot{K} = \sum_1^n \int_{\Omega_i} \{\dot{e}^T \nabla z + e^T \dot{\overline{\nabla z}} + (e^T \nabla z) \operatorname{div} v\} \, d\Omega_i \tag{7}$$

and

$$\sum_1^n \int_{\Omega_i} \{2 \nabla z^T \dot{\overline{\nabla z}} + e^T \dot{\overline{\nabla z}} + \dot{e}^T \nabla z + (\nabla z^T \nabla z + e^T \nabla z) \operatorname{div} v\} \, d\Omega_i = 0 \tag{8}$$

with the help of the following definitions:

$$\dot{e} \equiv \left. \frac{de}{dt} \right|_{t=0}$$

and

$$\dot{\overline{\nabla z}} \equiv \left. \frac{d(\nabla z)}{dt} \right|_{t=0}$$

It is derived from Refs. 6 and 11 that

$$\dot{\overline{\nabla z}} = \nabla \dot{z} - (\nabla v \ \nabla z) \tag{9}$$

where the matrix $\nabla v$ represents the gradient of velocity vector, and $\dot{e} \equiv \{\dot{x}_1, \dot{x}_2\}^T = \{v_1, v_2\}^T \equiv v$, in which $v_1$ and $v_2$ are velocity components along the $x_1$ and $x_2$ directions, respectively. Therefore, one has the following equality:

$$\sum_1^n \int_{\Omega_i} \left( \nabla z^T \dot{\overline{\nabla z}} + e^T \dot{\overline{\nabla z}} \right) d\Omega_i = \sum_1^n \int_{\Omega_i} (\nabla z^T \nabla \dot{z} + e^T \nabla \dot{z}) \, d\Omega_i - \sum_1^n \int_{\Omega_i} (\nabla z + e)^T (\nabla v \nabla z) \, d\Omega_i \tag{10}$$

Recall the variational formula for the torsion of an elastic hollow bar,[4] which is to find the solution $z \epsilon H$ such that the equality

$$\int_\Omega \nabla z^T \nabla \bar{z} \, d\Omega + \int_\Omega e^T \nabla \bar{z} \, d\Omega = 0 \tag{11}$$

is true for all $\bar{z} \epsilon H$, where $H$ is the kinematically admissible function space defined as $H \equiv \{\bar{z} \epsilon H^1(\Omega) \mid \bar{z} = 0$ on $\Gamma_0$ and $\dot{z} = \dot{q}$ on $\Gamma_0$ and $\bar{z} = q$ on $\Gamma_i\}$ for an arbitrary constant $q$, and $H^1(\Omega)$ is the Sobolev space of order one. Since $z \epsilon H$, $\dot{z} = 0$ on $\Gamma_0$ and $\dot{z} = \dot{q}$ on $\Gamma_i$, where $\dot{q}$ is also a constant. It can also be shown[11] that $\dot{z} \epsilon H^1(\Omega)$. Thus, the first term on the right in Eq. (10), which is the discretization form of Eq. (11) with $\bar{z} = \dot{z} \epsilon H$, is identical to zero. In other words, the relation of Eq. (10) can

be reduced to

$$\sum_1^n \int_{\Omega_i} \left( \nabla z^T \dot{\overline{\nabla z}} + e^T \dot{\overline{\nabla z}} \right) d\Omega_i$$

$$= - \sum_1^n \int_{\Omega_i} (\nabla z + e)^T (\nabla v \nabla z) d\Omega_i$$

Substituting the preceding result and the relation $\dot{e} = v$ into Eqs. (7) and (8) yields

$$\dot{K} = \sum_1^n \int_{\Omega_i} e^T \dot{\overline{\nabla z}} \, d\Omega_i + \sum_1^n \int_{\Omega_i} (v^T \nabla z + e^T \nabla z \text{div} v) d\Omega_i \quad (12)$$

and

$$\sum_1^n \int_{\Omega_i} e^T \dot{\overline{\nabla z}} \, d\Omega_i = \sum_1^n \int_{\Omega_i} \{ -2(\nabla z + e)^T (\nabla v \ \nabla z)$$

$$+ v^T \nabla z + (\nabla z^T \nabla z + e^T \nabla z) \ \text{div} v \} d\Omega_i \quad (13)$$

Finally, replacing the term with $(\cdot / \nabla z)$ in $\dot{K}$ by Eq. (13), one can express the shape design sensitivity of the torsional rigidity in terms of shearing stresses $\nabla z$, position vector $e$, and the velocity field $v$ in each individual element

$$\dot{K} = 2 \sum_1^n \int_{\Omega_i} \{ -(\nabla z + e)^T (\nabla v \nabla z)$$

$$+ v^T \nabla z + \left( \frac{\nabla z^T \nabla z}{2} + e^T \nabla z \right) \text{div} v \} d\Omega_i \quad (14)$$

Note that the foregoing equality is a linear functional of velocity field $v$. The stress function $z$ can be interpolated, according to the finite element method, as

$$z = Nz \quad (15)$$

where $N$ is a matrix of shape functions, and $z$ is the vector of nodal values. The position vector $e$ at any point in the element domain can be interpolated by the shape functions and the coordinates at the nodal points.[14] For a triangular element, the position vector is simply vector form

$$e = (x,y)^T = Lx \quad (16)$$

where $L$ is a matrix of area coordinates $L_i$, $(x_i, y_i)$ is the nodal coordinate, and $x$ is a vector of nodal coordinates.

The question of defining the velocity field remains. To be consistent with the finite element discretization, the velocities at the nodes may be chosen as independent unknowns denoted by nodal velocities. The velocity at any point within the element can then be expressed by the linear combination of shape functions and nodal velocities.[13,15] Note that the shape functions used for the stress function, position vector, and velocity may be different. As mentioned in Ref. 5, it is required that the continuity of the velocity field be at least $v \epsilon C^0(\Omega)$. It is well known that the displacement field defined in the constant stress triangle possesses $C^0(\Omega)$. Consequently, the linear shape functions can be adopted here to interpolate the velocity field within a triangle. Let the nodal velocities of a triangle, $(u_i, v_i)$ be defined as shown in Fig. 1.

The velocity components at any point within the triangular element are then given by a matrix form

$$v(x,y) = Lv \quad (17)$$

where $L$ is a matrix of area coordinates $L_i$. In general, it is not beneficial to treat all the nodal velocities as design variables. First, the optimum design may end up with too many design variables; second, such treatment might distort the finite element grid too much (unless certain geometric constraints associated with the mesh have been introduced). To limit the size of the optimal design problem, a function that relates the internal-nodal velocities and the velocities of the boundary nodes is usually introduced into the problem formulation. Of course, only boundary nodal velocities will be considered as the independent design variables.

As an example, the mesh of the grooved hollow shaft is arranged in such a way that any vector connecting the center O and the vertex of any outer boundary Q will pass a nodal point P of the inner boundary (see Fig. 2.) The angle between this vector and the $x$ axis will remain constant during the shape design process. For our study, the inner boundary is approximated by a polygon with 26 vertices, and the radial distance between O and P will be considered as a design variable. Therefore, there are 26 design variables for this problem. If it is necessary to vary the outer boundary, the radial distances between O and nodes on the outer boundary can be defined as design variables as well. All the nodal points between P and Q will be restricted to move along the radial direction O-P-Q. The ratios $\alpha_i$ of movements of nodes between P and Q (including P and Q) are assumed to be 1, 0.72, 0.49, 0.3, 0.14, and 0.0. In other words, if node P moves one unit inward, then the adjacent node will move 0.72 unit inwards as well, etc. Finally, it is concluded that the internal velocities of node k, $v_k$, can be expressed as a function of the nodal velocities $b_i$ of the boundary node i,

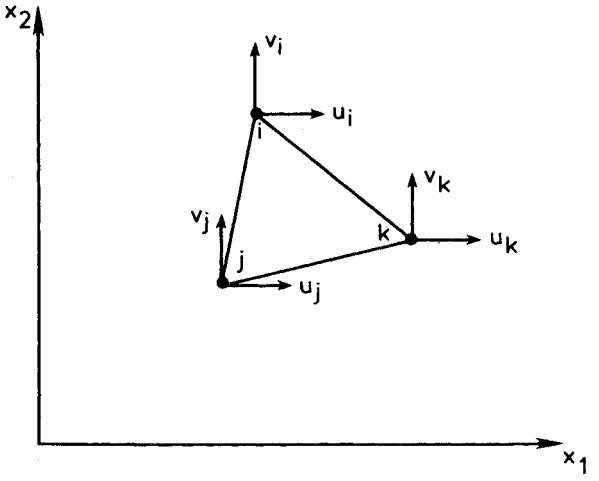


**Fig. 1 Nodal velocities of a triangular element.**

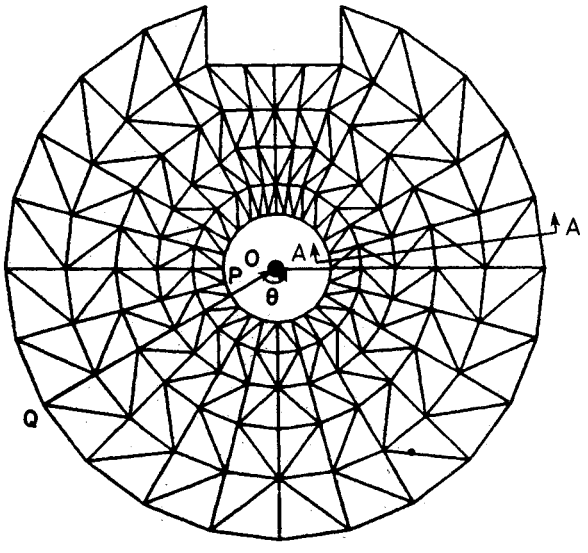


**Fig. 2 Finite element model (coarse mesh).**

through a transformation coefficient $a_i$ $(\alpha_{ik},\theta_i)$,

$$v_k = a_i(\alpha_{ik},\theta_i)\cdot b_i$$

where $\alpha_{ik}$ is the ratio of the nodal movements between internal node k and boundary node i, and $\theta_i$ is the angle of moving direction associated with the boundary node i. Substituting the preceding relation into Eq. (17), the velocity at any point can be written in terms of $\alpha_{ik}$, $\theta_i$, and the nodal velocities at the boundary nodes:

$$v = LAb$$

Note that the nodal velocities $b$ along the boundary are exactly defined as the perturbations of the design variables $\delta d$, i.e.,

$$b = \delta d$$

Thus

$$v = LA\delta d \tag{18}$$

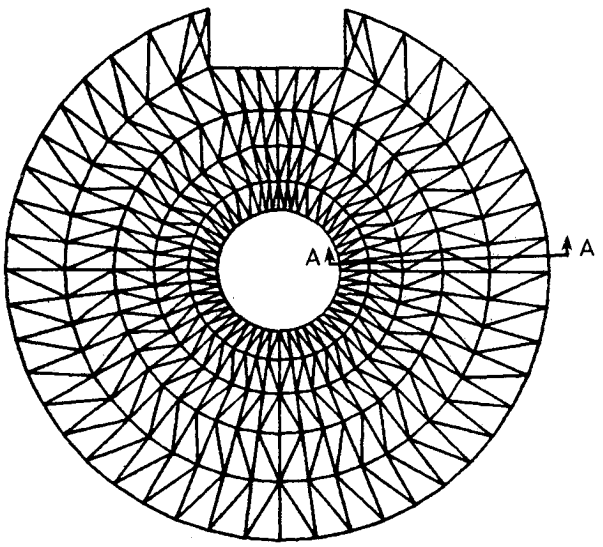


**Fig. 3 Finer finite element mesh for shaft with keyway.**

Substituting Eqs. (15), (16), and (18) into Eq. (14), one can perform the integration to obtain the shape design sensitivity of torsional rigidity over discretized elements without much difficulty.[13] Finally, the shape design sensitivity of torsional rigidity $\dot{K}$ can be presented by the following vector product:

$$\dot{K} = \ell^T \delta d$$

where $\ell$ is the sensitivity vector. Now that the problem is finite dimensional, any well-known gradient-based mathematical programming technique can be employed to find the optimum shape iteratively.

## III. Numerical Results and Discussions

### Shape Design Sensitivity

The shape design sensitivity of torsional rigidity for a grooved hollow shaft is the first example to be investigated. The material is assumed isotropic. The radius of the outer boundary is set as 2.0 units. The radii of the hole are varied from 0.4 to 0.95 units. The width and depth of the keyway are 1.0 and 0.5 units, respectively. Only the contour of the hole is pertubed. Linear shape functions are used for the finite element analysis. Two kinds of meshes are considered: a coarse mesh with 153 nodes and 252 triangular elements, as shown in Fig. 2, and a finer mesh with 287 nodes and 474 triangular elements, as shown in Fig. 3. For comparison with Eq. 14, the design sensitivity of torsional rigidity is also calculated by using the following equation[4]

$$\dot{K} = \int_{\Gamma_i} \left(\frac{\partial z}{\partial n}\right)^2 Vn\,ds \tag{19}$$

The above equation is derived based on Eq. (4), which does not consider the effects of discontinuities of $e^T\nabla z$ and internal-nodal movements. The sensitivity results corresponding to different meshes are listed in Table 1. It is noted that the design sensitivity calculated by using Eq. (19) is acceptable when the radius of the hole is large. However, neither the coarse nor finer mesh obtains satisfactory results when the radius becomes smaller. To have a better under-

**Table 1 Shape design sensitivity analysis**

| Direct difference | | Conventional method, Eq. (19) | | Improved method, Eq. (14) | |
|---|---|---|---|---|---|
| Radius, $r$ | $K(b+\delta b)$-$K(b)$ (1) | $\dot{K}\delta b$ (2) | $\frac{(2)-(1)}{1}\times\%$ | $\dot{K}\delta b$ (3) | $\frac{(3)-(1)}{1}\times\%$ |
| | | Coarse mesh | | | |
| 0.4 | $0.1058026\times10^{-3}$ | $0.1566808\times10^{-2}$ | 1380.88 | $0.9636332\times10^{-4}$ | −8.92 |
| 0.45 | $0.6965585\times10^{-3}$ | $0.2317506\times10^{-2}$ | 232.71 | $0.6825605\times10^{-3}$ | −2.01 |
| 0.6 | $0.4099872\times10^{-2}$ | $0.6262908\times10^{-2}$ | 52.76 | $0.4060712\times10^{-2}$ | −0.96 |
| 0.8 | $0.1480705\times10^{-1}$ | $0.1799805\times10^{-1}$ | 21.55 | $0.1408688\times10^{-1}$ | −0.81 |
| 0.95 | $0.3074586\times10^{-1}$ | $0.3529341\times10^{-1}$ | 14.79 | $0.3049462\times10^{-1}$ | −0.82 |
| CPU time (DEC-10) | | 2.91 s | | 5.56 s | |
| | | Finer mesh | | | |
| 0.4 | $0.3982522\times10^{-3}$ | $0.1519077\times10^{-2}$ | 281.44 | $0.4387125\times10^{-3}$ | 10.16 |
| 0.45 | $0.9993966\times10^{-3}$ | $0.2252647\times10^{-2}$ | 125.40 | $0.1033991\times10^{-2}$ | 3.46 |
| 0.6 | $0.4446395\times10^{-2}$ | $0.6117125\times10^{-2}$ | 37.58 | $0.4449391\times10^{-2}$ | 0.07 |
| 0.8 | $0.1530113\times10^{-1}$ | $0.1761505\times10^{-1}$ | 15.12 | $0.1521112\times10^{-1}$ | −0.59 |
| 0.95 | $0.3145241\times10^{-1}$ | $0.3450927\times10^{-1}$ | 9.72 | $0.3121946\times10^{-1}$ | −0.74 |
| CPU time (DEC-10) | | 6.79 s | | 10.78 s | |

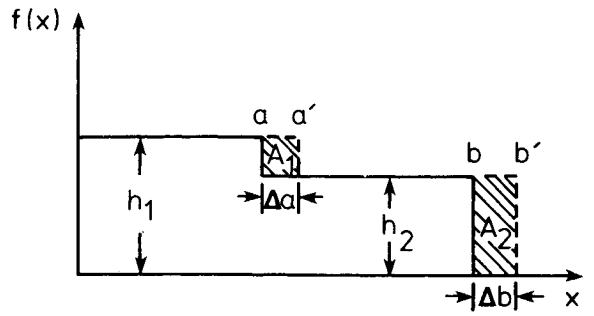


Fig. 4 Domain variation of a functional with step function.

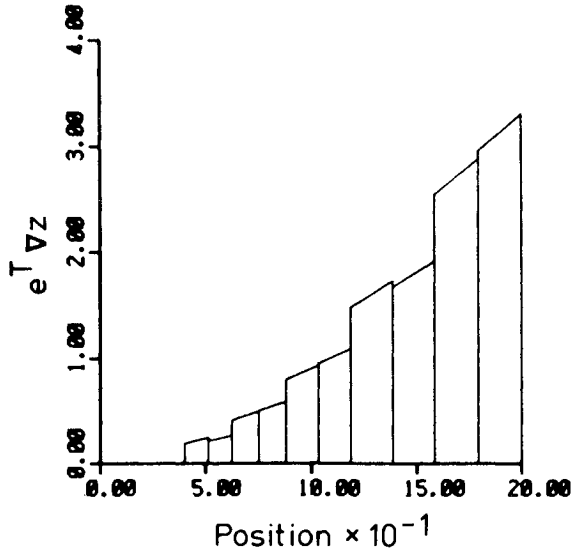


a) Coarse mesh.

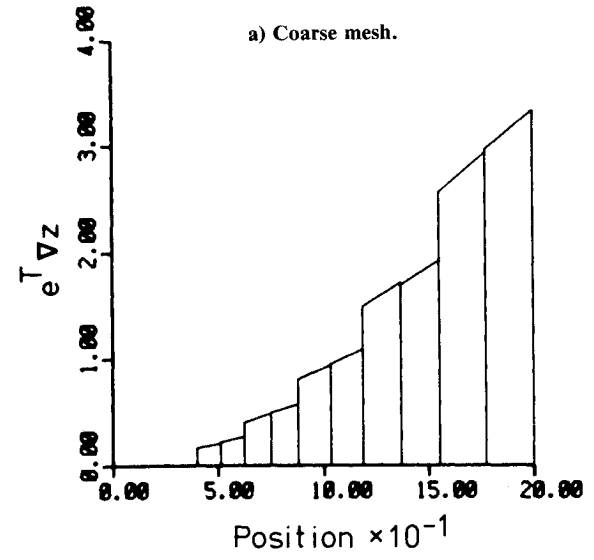


b) Fine mesh.

Fig. 5 Distribution of $e^T \nabla z (r = 0.4)$.

standing of this, it is helpful to study the following example:

*Example*: A step function with two fixed constants $h_1$ and $h_2$ is given as:

$$f(x) = \begin{cases} h_1, & 0 \le x < a \\ h_2, & a \le x \le b \end{cases}$$

Let points $a$ and $b$ move to $a'$ and $b'$ by $\Delta a$ and $\Delta b$ units,

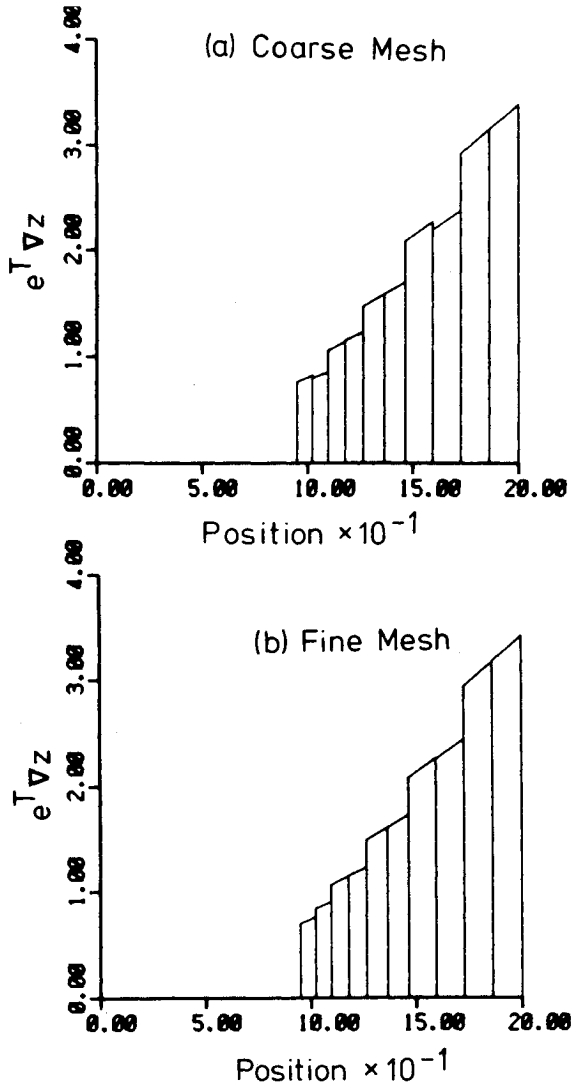


Fig. 6 Distribution of $e^T \nabla z (r = 0.95)$.

respectively. Find the corresponding change in the functional:

$$\psi = \int_0^b f(x)\,dx$$

The dotted line shown in Fig. 4 denotes the "deformed" function. It is clear that the variation of the above functional, due to the nodal movements, will be the summation of shaded areas $A_1 = (h_1 - h_2)\,\Delta a$ and $A_2 = h_2\,\Delta b$. However, the material derivative, Eq. (4), can account for the perturbation of the functional with an amount of $h_2 \Delta b$ only. The error induced by the movement of internal node can be significant, unless the ratio $A_1/A_2$ is small, which is true provided $\Delta a \ll \Delta b$ and/or $(h_1 - h_2) \ll h_2$.

Since linear shape function is used for analysis, the term $e^T \nabla z$ in Eq. (5) corresponding to $f(x)$ in the example possesses discontinuities across the element boundaries, as shown in Figs. 2 and 3 along the section AA (indicated in Figs. 2-3). Similar patterns of stress distributions are also observed along different radial sections.[13] In Fig. 5, where the radius is taken as $r = 0.4$, the jump of the function along the inner boundary has similar or even less magnitude compared to the jumps along the element boundaries. On the other hand, the function along the inner boundary displays a significant jump compared to the jumps along the element boundaries as shown in Fig. 6, when $r = 0.95$. In other words, the jump along the inner boundary, with $r = 0.95$,

contributes a bigger fraction of the domain variation of functionals than in the case of $r=0.4$. Thus, recalling the example, it is possible, in the case of $r=0.95$, to achieve acceptable accuracy in the shape design sensitivity result analyzed by using Eq. (4), though the effect of movement of the internal nodes is not considered in the formulation of Eq. (4).

It is obvious that the current approach provides vast improvement. It also confirms that the internal-nodal movements do have significant effect on the shape design sensitivity analysis. Table 1 indicates the CPU time for shape design sensitivity, which includes two finite element analyses and one evaluation of gradient, Eq. (14) or (19). It shows that the conventional technique, which employs Eq. (19) without considering the effect of internal-nodal movements, has an advantage in computational efficiency over the current technique.

It can be seen from Table 1 that by using the proposed method the accuracy of shape design sensitivity analysis for the studied example is almost irrelevant to the mesh pattern. The results of Table 1 show that the accuracy of shape design sensitivity differs depending on the radius. This may be attributed in part to the nonlinearity of the shape design problem. However, it is still a somewhat open question.

The next subject for study is the change of the domain functional caused by the internal-nodal movements while the shape of the domain where the functional is defined remains unperturbed. An interesting application of such a case is the problem of meshing optimization,[16] which can minimize the numerical error by relocating the internal nodes. The total potential energy is one of the widely used error measurements for finite element analysis.[17] It is known that the total potential energy is proportional to the torsional rigidity of a torsional bar, according to the Clapeyron's theorem. Thus, Eq. (14) can be used directly to calculate the design sensitivity of the numerical error which, of course, corresponds to the finite element analysis of an elastic hollow bar in torsion.

The finite element model to be used is shown in Fig. 7. Only one-quarter of the whole cross section is considered because of symmetry. These are 24 triangular elements and 20 nodes. Again, linear shape functions are used for the finite element analysis. For simplicity, the $(r,\theta)$ coordinate system is used to denote positions of nodes. During the perturbation, the coordinate $r$'s of nodes 1-5 and 16-20 are fixed as five units and two units, respectively, and the $\theta$'s of nodes 1, 6, 11, and 16 and 5, 10, 15, and 20 are fixed as 0 and 90 deg, respectively. The rest of the coordinates, 22 in all, are considered as design variables. Since there is no boundary perturbation, there is no normal velocity along the boundary. Therefore, even with internal-nodal movements, no change in torsional rigidity (or total potential energy) is found, according to Eq. (19), which does not take in account the movement of discontinuities. On the other hand, the satisfactory design sensitivity information can be obtained by using the improved derivation [Eq. (14)], as shown in Fig. 8. The x and y axes of the figure denote various percentage changes in design variables and changes in the torsional rigidity, respectively. It can be clearly seen that the predicted change in the numerical error of the finite element analysis is closer to the value calculated by the direct difference when the change of nodal coordinates is smaller. This is because Eq. (14) represents only the first-order variation and the problem is nonlinear.

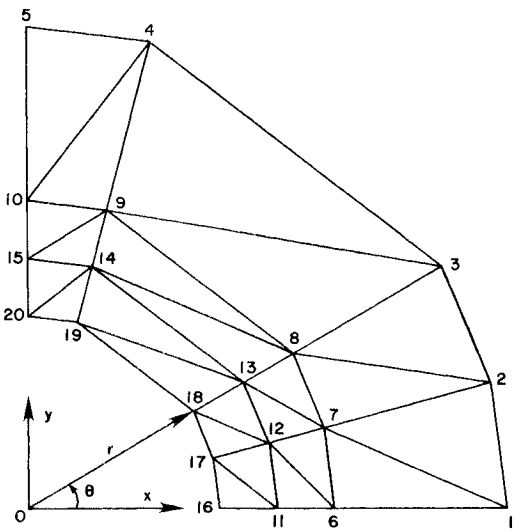


Fig. 7 An example for meshing optimization.

### Shape Optimal Design

Once the sensitivity analysis is done accurately, it is not difficult to determine the optimum shape using any gradient-based mathematical programming technique.

Again, considering the hollow shaft with a groove for keyway as an example, the optimum shape is obtained by choosing cross-sectional geometry of the inner boundary such as to maximize the torsional rigidity. The cross-sectional area is restricted to 11 units. The initial value estimated for the inner boundary is a circle with a radius of 0.45 unit. The optimum design is carried out by using the

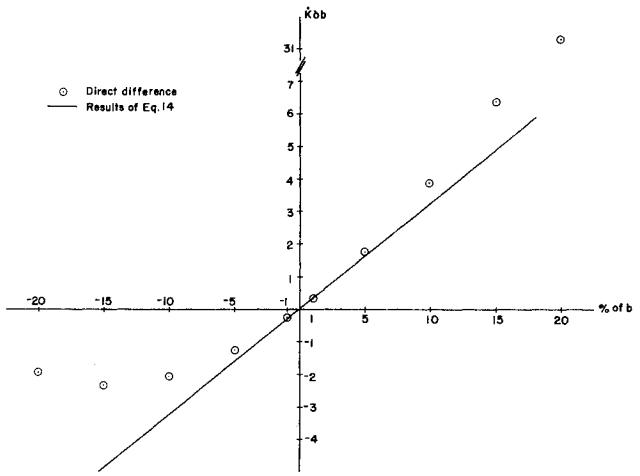


Fig. 8 The shape design sensitivity of torsional rigidity with respect to perturbations of design variables.

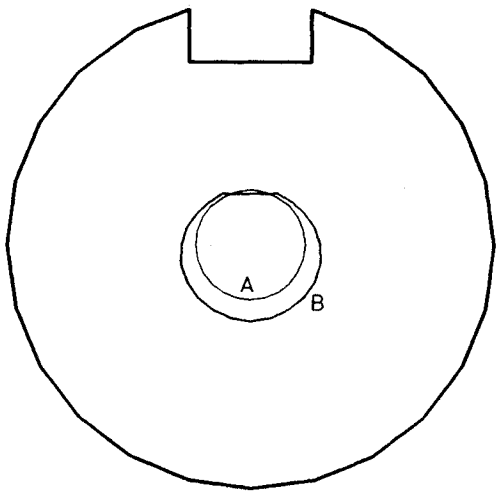


Fig. 9 Optimum shape of hollow bar with keyway, Eq. (14), with coarse mesh. A curve: initial design; B curve: optimum design.

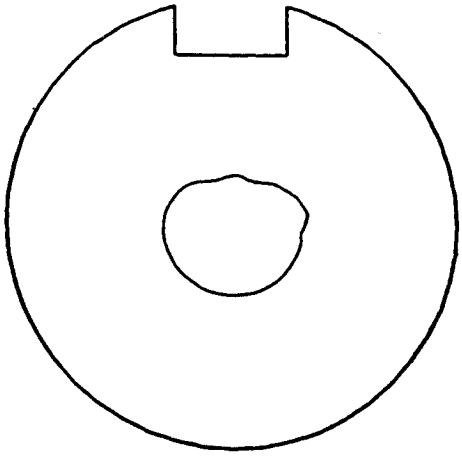

Fig. 10 Contour of inner boundary at 17th iteration, Eq. (19), with finer mesh.

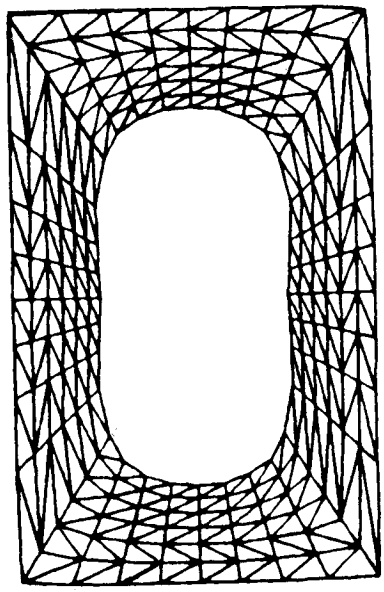

Fig. 11 Optimum shape for a torsional bar, Eq. (19), with coarse mesh.

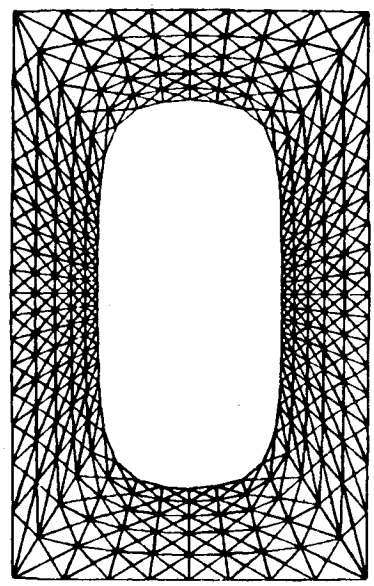

Fig. 12 Optimum shape for a torsional bar, Eq. (19), with finer mesh.

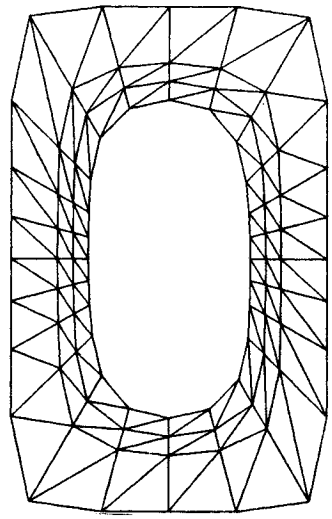

Fig. 13 Optimum shape for a torsional bar.

Table 2 Numerical results for a torsional bar with hollow cross section

| | No. of FE elements and nodes | No. of design variables | No. of iterations | Optimum torsional rigidity | Constraint (area = 110 units) |
|---|---|---|---|---|---|
| Coarse grid (Fig. 11) | 384 and 224 | 64 | 755 | 2826.9 | 107.8 |
| Finer grid (Fig. 12) | 960 and 528 | 96 | 410 | 2820.8 | 106.7 |
| New grid (Fig. 13) | 144 and 96 | 48 | 191 | 2830.4 | 110.38 |

linearization method.[18] The optimum shapes corresponding to the coarse mesh shown in Fig. 2 are plotted in Fig. 9. It takes 16 iterations and 70.4 CPU s on a DEC-10 to converge. For comparison purposes, the conventional approach [Eq. (19)] is also employed to perform the optimization based on the finer mesh. The algorithm fails to converge and stops after 17 iterations, due to failure of line search. The shape of the cross section at the seventeenth iteration is shown in Fig. 10.

As a final example, the shape optimization of the elastic hollow bar in torsion is resolved here. Both the outer and inner boundaries of the hollow bar are to be designed for maximum torsional rigidity. In addition to the constraint on the amount of material available, the cross section of the bar is required to be in a 10 × 16 unit rectangular housing. The optimum shape shown in Fig. 13 is solved by the proposed technique of Eq. (14). The same problem has been solved in Ref. 4 by the conventional technique based on two different

meshes. One mesh has 384 elements, 224 nodes, and 64 design variables, as shown in Fig. 11. The other mesh has 960 elements, 528 nodes, and 96 design variables, as shown in Fig. 12. It is found that the values of optimum torsional rigidity are very close for these two meshes; however, the optimum contours of the inner boundaries show significant difference. The boundary with the coarse finite element mesh is peanut-shaped. On the other hand, the optimum inner boundary of the finer element mesh is oval-shaped, similar to the results shown in Fig. 13. Reference 4 indicates that the improved stress evaluation that yields a better approximation of design sensitivity coefficients has caused the deviation.

The numerical results for the three outlined cases are listed in Table 2. Note that with fewer elements, the optimum solution can be obtained by using the proposed method with fewer iterations. Moreover, the new method provides better design because the value of the torsional rigidity is higher and the equality constraint is better satisfied.

## IV. Conclusion and Remarks

One of the computational differences between the shape optimum design and the conventional optimum design is that the mesh regridding during design iteration is necessary to prevent undesirable distortion of the grid mesh. The two ingredients in a shape optimum design algorithm—finite element discretization and mesh regridding—should be considered together. The material derivative provides a very powerful means to derive the shape design sensitivity. However, the continuity requirement for the integrand of domain functional has to be investigated before the material derivative can be properly applied.

The effect of internal-nodal movements, which is associated with the mesh regridding, on the shape design sensitivity has been investigated carefully in this presentation. To obtain a better numerical scheme, it is concluded that the internal-nodal movements should be considered in analyzing shape design sensitivity. The preceding discussion also clarifies the observation[19] that using the boundary element method as an analytical tool benefits the shape optimum design since there is no internal node at all for the boundary element method.

A new approach is developed and presented by using a different form of material derivative, which requires the velocity field over each individual element. The improvement of the shape design sensitivity is very impressive. Even with the coarse grid and limited number of design variables, the new approach still performs very well. While the specific problem concerns optimization of elastic bars subjected to pure torsion, the basic concepts introduced in this presentation are quite general.

This presentation has focused on the numerical implementation of the material derivative (or speed) method for shape design sensitivity. To reach a compromise between computational cost and numerical accuracy, a suggestion is offered: further study to combine a mesh optimization scheme monitoring cross-element discontinuity and the conventional method [e.g., Eq. (19)] for shape design sensitivity analysis.

## Acknowledgments

The authors are pleased to acknowledge partial support of this research by the Institute for Computational Applied Mechanics, Old Dominion University.

## References

[1]Botkin, M. E., "Shape Optimization of Plate and Shell Structures," AIAA Paper 81-0553, April 1981.

[2]Zienkiewicz, O. C. and Campbell, J. S., "Shape Optimization and Sequential Linear Programming," *Optimum Structural Design,* edited by R. H. Gallagher and O. C. Zienkiewicz, John Wiley & Sons, New York, 1973, pp. 109-126.

[3]Ramakrishnan, C. V. and Francavilla, A., "Structural Shape Optimization Using Penalty Functions," *Journal of Structural Mechanics,* Vol. 3, No. 4, 1975, pp. 403-432.

[4]Hou, J. W., Haug, E. J., and Benedict, R. L., "Shape Optimization of Elastic Bars in Torsion," *Sensitivity of Functionals, Lecture Notes in Mathematics,* Vol. 1086, Springer-Verlag, New pp. 31-55.

[5]Zolesio, J. P., "The Material Derivative (or Speed) Method for Shape Optimization," *Optimization of Distributed Parameter Structures,* Vol. II, edited by E. J. Haug and J. Cea, Sijthoff & Noordhoff, Alphen aan den Rijn, The Netherlands, 1981, pp. 1101-1164.

[6]Gelfand, J. M. and Fomin, S. V., *Calculus of Variation,* Prentice-Hill, Englewood Cliffs, NJ, 1963.

[7]Haug, E. J., Choi, K. K., and Komkov, V., *Structural Design Sensitivity Analysis,* Academic Press, Orlando, FL, 1986.

[8]Taylor, A. E. and Mann, W. R., *Advanced Calculus,* 2nd ed., Xerox Corporation, MA, 1972.

[9]Cea, J., "Numerical Methods of Shape Optimal Design," *Optimization of Distributed Parameter Structures,* Vol. II edited by E. J. Haug and J. Cea, Sijthoff & Noordhoff, Alphen aan den Rijn, The Netherlands, 1981, pp. 1061-1099.

[10]Rousselet, B., "Implementation of Some Methods of Shape Optimal Design," *Optimization of Distributed Parameter Structures,* Vol. II, edited by E. J. Haug and J. Cea, Sijthoff & Noordhoff, Alphen aan den Rijn, The Netherlands, 1984, pp. 1209-1284.

[11]Angrand, F., "Optimum Design for Potential Flows," *International Journal of Numerical Methods in Fluids,* Vol. 3, Feb. 1983, pp. 265-282.

[12]Choi, K.K and Seong, H. G., "A Domain Method for Shape Design Sensitivity Analysis of Built-Up Structures," *Computer Methods in Applied Mechanics and Engineering,* to appear, 1986.

[13]Chen, J. L., *Shape Optimization for Elastic Hollow Bars in Torsion,* M. S. Thesis, Department of Mechanical Engineering and Mechanics, Old Dominion University, Norfolk, VA, April 1984.

[14]Zienkiewicz, O. C., *The Finite Element Method,* 3d Ed. McGraw-Hill Book Co., New York, 1977.

[15]Braibant, V. and Fleury, C., "Shape Optimal Design: A Performing C.A.D. Oriented Formulation," AIAA Paper 84-0857, May 1984.

[16]Liniecki, A. and Yun, J., "Finite Element Triangular Meshing Optimization for Pure Torsion," *International Journal for Numerical Methods in Engineering,* Vol. 19, No. 6, 1983, pp. 929-942.

[17]McNeice, G. M, and Marcal, P. V., "Optimization of Finite Element Grids Based on Minimum Potential Energy," Division of Engineering, Brown University, Providence, RI, Tech. Rept. No. 7, June 1971.

[18]Choi, K. K., Haug, E. J., Hou, J. W., and Sohoni, V. N., "Pshenichny's Linearization Method for Mechanical System Optimization," *Journal of Mechanics, Transmissions, and Automation in Design,* Vol. 105, March 1983, pp. 97-103.

[19]Mota Soars, C. A., Rodrigues, H. C., Oliveira Faria, L. M., and Haug, E. J., "Optimization of the Shape of Solid and Hollow Shafts Using Boundary Elements,"*Boundary Elements,* edited by C. A. Brebbia, T. Futagami, and M. Tanaka, Springer-Verlag, Tokyo, 1983, pp. 883-890.